IEEE Access
Multidisciplinary ⋮ Rapid Review ⋮ Open Access Journal

Received June 22, 2018, accepted August 18, 2018, date of publication August 27, 2018, date of current version September 21, 2018.

Digital Object Identifier 10.1109/ACCESS.2018.2867349

Development of Energy-Based Brittleness Index for Sandstone Subjected to Freeze-Thaw Cycles and Impact Loads

JIAN ZHANG[1,2], (Member, IEEE), HONGWEI DENG[1], JUNREN DENG[1], AND BO KE[3]
[1]School of Resources and Safety Engineering, Central South University, Changsha 410083, China
[2]School of Civil, Environmental and Mining Engineering, The University of Adelaide, Adelaide, SA 5005, Australia
[3]School of Resource and Environment Engineering, Wuhan University of Technology, Wuhan 430070, China

Corresponding authors: Junren Deng (csudjr@163.com) and Bo Ke (kebo53@163.com)

This work was supported in part by the Fundamental Research Funds for the Central Universities of Central South University under Grant 2015zzts082 and in part by the National Natural Science Foundation of China under Grants 51774323 and 51874352. The work of J. Zhang was supported by the Chinese Scholarship Council to the joint Ph.D. at the University of Adelaide.

ABSTRACT As one of the most important parameters of rock materials, brittleness is affected by external conditions such as temperature and dynamic disturbances. However, there is no universal criterion for brittleness. In this paper, the brittleness of sandstone subjected to rapid freeze–thaw (F–T) cycles and impact loads are investigated. The 25 specimens were subjected to different F–T cycles and impact loads and then investigated. It was found that the dynamic strength and Young's modulus of the specimens decrease, whereas porosity increases after the application of F–T cycles. The dynamic stress–strain curves demonstrated that after the peak point, the rock sample first exhibited class I behavior and then class II behavior. Previous studies implied that the brittleness index based on the pre-peak stress–strain characteristics was not sufficient to describe the rock fracture. Two brittleness indices based on the pre-peak and post-peak strain energy were thus derived using the complete dynamic stress–strain characteristics of rock samples. The two brittleness indices were strongly correlated with the physical parameters, such as porosity and mechanical parameters, including peak stress and dynamic modulus.

INDEX TERMS Sandstone, energy, brittleness, freeze-thaw, impact load.

I. INTRODUCTION

Rocks are often exposed to different external environments such as extreme temperature and impact loads. The behavior of rocks differs from each other owing to their external conditions. The mechanical and physical properties of different rocks subjected to F-T cycles have been studied by Altindag *et al.* [1], Fener and İnce [2], Karaca *et al.* [3], Momeni *et al.* [4], and Nicholson and Nicholson [5]. The results showed that with the increase in the number of F-T cycles, rocks exhibit deterioration and degradation to some extent in terms of the strength, P wave velocity and mass. Several studies have already focused on the mechanical properties of rocks under impact loads [6]–[8]. However, only a few studies have investigated the degradation of rocks under the combined effects of F-T cycles and impact loads.

Brittleness is an important mechanical property of intact rocks owing to its strong influence on the failure process of a rock mass, which is relevant to civil activities such as tunneling and mining. The concept of brittleness corresponds to the fracture characteristics of hard and strong materials. Rock behavior (see Figure 1) can be divided into class I behavior or class II behavior based on the classification proposed by Wawersik and Fairhurst [9]. However, the concept of brittleness has not yet been defined by a universal criterion. Brittleness can be treated as an intrinsic material property or as the material behavior under an external loading system that contributes additional energy to the failure process [10]. In the past years, different brittleness criteria have been proposed to characterize rock behavior under compression. Table 1 summarizes the existing brittleness criteria.

Brittleness indices can be expressed using different formulae, based on which parameters have been adopted to define the brittleness index. However, a brittleness index may be suitable for a certain situation but not for another. For example, the brittleness indices based on elastic and plastic strain (B_1–B_5) are found to be insufficient to describe the

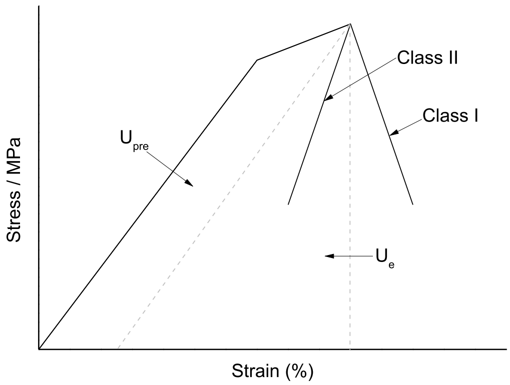

FIGURE 1. **Scheme of representative stress-strain curves for two classes of rock failure behavior in uniaxial compression [9].**

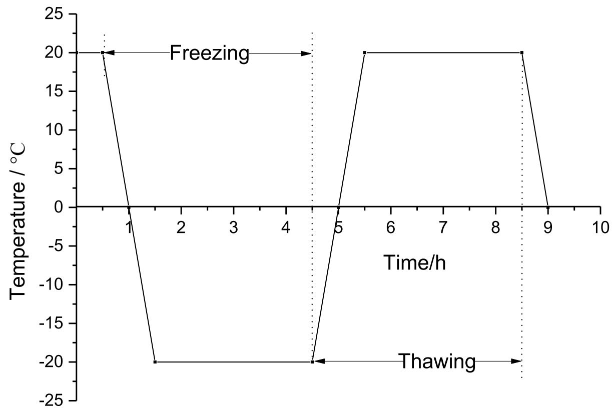

FIGURE 2. **Temperature versus time curve.**

failure behavior of rock [10]. In some cases, it is necessary to also consider the pre-peak and post-peak characteristics. By extension, brittleness indices based on strength (B_6–B_9), mineral composition (B_{20}–B_{23}), Young's modulus and Poisson' ratio (B_{24}–B_{29}), Mohr's envelope (B_{30}), hardness (B_{31}), porosity (B_{32}) and percentage of fines (B_{33}–B_{34}), among others are not sufficient to describe the rock behavior precisely. Brittleness indices, i.e. B_{12}, B_{13} and B_{14}, which based on pre-peak and post-peak strain energies, showed good correspondence with mechanical properties such as peak stress, crack damage stress and tangent Young's modulus. The author also demonstrates that brittleness indices B_{10} and B_{11} were not able to correlate well with the three pre-peak parameters. From the discussion above, it can be seen that the brittleness indices based on both pre-peak and post-peak energy can characterize the rock behavior.

In this study, 25 sandstone samples under F-T cycles and impact load were analyzed. Porosity and dynamic stress-strain curves were investigated. Based on the classification of Wawersik and Fairhurst [9], two brittleness indices were proposed; these were defined as the ratio of the energy consumed during class I behavior and the elastic energy and that during class II behavior and the elastic energy. Finally, the correlations between the proposed brittleness indices and F-T cycles, porosity, peak stress and Young's modulus were obtained.

II. MATERIALS AND METHODS

A. SPECIMEN PREPARATION

Porous sandstone formed underneath seabed or land contains a large amount of intergranular pore spaces. The mechanical behavior of sandstones has been investigated previously [37]. To perform this research, cylindrical sandstone samples were cored from a rock block. The diameter of each specimen was 50 mm, and their aspect ratio (i.e., length to diameter) was maintained at 1 [38] for dynamic tests. The diameter of sample was more than 20 times larger than the grain size, thereby satisfying the specimen size recommended by the International Society for Rock Mechanics (ISRM). The surface of the specimens was prepared to be smooth and straight. In order to reduce the friction, surface roughness of the cylindrical samples is less than 0.02mm and the end surfaces perpendicular to its axis is less than 0.001 radians. The rock samples corresponded to fine grain-size rock having a dry density of 2.21 g/cm^3. Before the experiment, water-physical properties of the selected sandstones were determined, and the results are presented in Table 2.

B. EXPERIMENTAL METHODS

In total, 25 specimens were used. These specimens were divided into 5 groups with each group comprising 5 specimens. For each group, rapid F-T tests were conducted, and the corresponding rate of change of temperature is shown in Figure 2. In this study for freezing and thawing, temperatures of −20°C and 20°C were adopted respectively according to the average highest and lowest temperatures of the rock block location. A TDS–300 F-T machine with a lowest freezing temperature of −40°C and a highest thawing temperature of 20°C was used to conduct the F-T treatment of the samples. The F-T cycles of each group were repeated 0, 20, 60, 100 and 140 times. Each F-T cycle lasted 8 h (i.e., 4 h freezing and 4 h thawing) according to the "Test Methods of Rock for Highway Engineering" proposed by the Ministry of Transport of the People's Republic of China.

Nuclear Magnetic Resonance (NMR) is a non-destructive technology to measure the characteristics of a rock's internal structure [39], such as pore size distribution and permeability [40]–[42], based on the measurement of signal decay of hydrogen atoms in a fully saturated rock sample. The NMR analysis system is suitable to measure the porosity of saturated specimens. In this study, a low field NMR analysis system (type AniMR-150) manufactured by Niumai Electric Technology Company was used. NMR tests were conducted after the F-T cycles for each specimen to measure the porosity. Figure 3 shows the T_2 relaxation time and accumulative porosity curve based on the results of T_2 relaxation time. A final porosity of 7.197% was obtained from the results shown in Figure 3.

TABLE 1. Summary of existing brittleness indices definitions.

Measurement methods	Formula	Description	References
Based on strain	$B_1 = \varepsilon_r/\varepsilon_e$	ε_r and ε_e are the reversible strain and total strain at the failure point, respectively	[12]
	$B_2 = \frac{\varepsilon_p}{\varepsilon_e}$ $B_3 = \frac{\varepsilon_{tp}}{\varepsilon_e}$	ε_p, ε_e and ε_{tp} are the elastic strain, post-peak strain and total irreversible post-peak strain, respectively	[13]
	$B_4 = \frac{\varepsilon_f^p - \varepsilon_c^p}{\varepsilon_c^p}$	ε_f^p is the plastic strain at which the friction strength is fully mobilized, ε_c^p is the plastic strain at which cohesive strength reduces to its residual value	[14]
	$B_5 = \varepsilon_{ir} * 100$	ε_{ir} is the irreversible longitudinal strain	[15]
Based on strength	$B_6 = \frac{\sigma_c - \sigma_t}{\sigma_c + \sigma_t}$	σ_c and σ_t are the compressive and tensile strengths, respectively	[12]
	$B_7 = \frac{\tau_p - \tau_r}{\tau_p}$	τ_p is the peak shear strength, τ_r is the residual shear strength	[16]
	$B_8 = \frac{\sigma_c \sigma_t}{2}$ $B_9 = \sqrt{\sigma_c \sigma_t/2}$	σ_c and σ_t are the compressive and tensile strengths, respectively	[17, 18]
Based on energy	$B_{10} = U^e/U^{peak}$	U_e and U_{peak} are the elastic energy and strain energy until peak stress, respectively	[12]
	$B_{11} = {U_{pre}}/{U_e}$	U_e is the elastic energy, U_{pre} is the pre-peak energy	[19]
	$B_{12} = {U_e}/{U_{total}}$ $B_{13} = {U_e}/{U_{post}}$ $B_{14} = {U_{peak}}/{U_{total}}$	U_e is the elastic energy, U_{total} is the total fracture energy, U_{post} is the post-peak energy	[11]
	$B_{15} = M - {E}/{M}$ $B_{16} = {E}/{M}$	E is the elastic modulus and M is the post-peak modulus	[10]
	$B_{17} = {M}/{E} + M$ $B_{18} = {M}/{E}$	E is the elastic modulus and M is the post-peak modulus	[20-24]
	$B_{19} = \frac{H}{E}$	H is the hardening modulus and E is the Young's modulus	[25]
Based on mineral composition	$B_{20} = \frac{F_{Qtz}}{F_{Qtz} + F_{Cb+Cly}}$	F indicates fraction, mineral abbreviations are Qtz = quartz, Cb = carbonate, Cly = clay, Dol = dolomite, Cal =calcite	[26]
	$B_{21} = \frac{F_{Qtz+Dol}}{F_{Qtz+Dol} + F_{Cal+Cly+TOC}}$		[27]
	$B_{22} = \frac{F_{Qtz+Cb}}{F_{Qtz+Cb} + F_{Cal+TOC}}$		[28]
	$B_{23} = \frac{w_{QFP} F_{QFP}}{w_{QFP} F_{QFP} + w_{Cb} F_{Cb} + w_{ClyTOC} F_{ClyTOC} + w_\emptyset \emptyset}$	w_{QFP}, w_{Cb}, w_{ClyTOC}, and w_Φ are weighting factors that range between 0 and 1 and may be adapted to deformation conditions	[25]
Based on Young's modulus and Poisson' ratio	$B_{24} = \frac{E - E_{min}}{E_{max} - E_{min}}$	E is the elastic modulus, E_{min} and E_{max} are the maximum and minimum Young's moduli, respectively	[29]
	$B_{25} = \frac{1}{2}\left[\frac{E - E_{min}}{E_{max} - E_{min}} + \frac{v_{max} - v}{v_{max} - v_{min}}\right]$	E_{min} and E_{max} are the maximum and minimum Young's moduli, respectively; v_{max} and v_{min} are the maximum and minimum Poisson's ratio, respectively	[30]
	$B_{26} = \frac{E}{v}$	E and v are the Young's modulus and Poisson's ratio, respectively	[31]
	$B_{27} = \frac{E\rho}{v}$	E and v are the Young's modulus and Poisson's ratio, respectively; ρ is the rock density	[32]
	$B_{28} = \frac{\lambda + 2\mu}{\lambda}$	λ is Lame's first parameter and μ is the shear modulus	[33]
	$B_{29} = \frac{E}{\lambda}$	E is Young's modulus and λ is Lame's first parameter	[34]
Based on Mohr's envelope	$B_{30} = sin\theta$	θ is the internal friction angle	[12]
Based on hardness	$B_{31} = \frac{H_\mu - H}{K}$	H_μ is the micro-indentation hardness, H is the macro-indentation hardness and K is a constant	[12]
Based on porosity	$B_{32} = -1.8748 * \emptyset + 0.9679$	$\emptyset$ is the neutron porosity	[35]
Based on the percentage of fines	$B_{33} = \frac{F_{max}}{P}$	F_{max} is the maximum applied force and P is the corresponding penetration	[36]
	$B_{34} = q\sigma_c$	q is percentage of fines (-28 mesh) formed in protodyakonov impact test, σ_c is uniaxial compression strength	[12]

TABLE 2. Water-physical properties of selected samples.

Specimen	Dry weight	Wet weight	Saturation weight	Water absorption	Saturation ratio	Saturation coefficient
1	428.77 g	449.18 g	460.31 g	4.76%	7.36%	0.65
2	417.67 g	438.08 g	448.51 g	4.89%	7.38%	0.66
3	429.65 g	449.88 g	461.00 g	4.71%	7.30%	0.65
Average	425.36 g	445.71 g	456.61 g	4.78%	7.35%	0.65

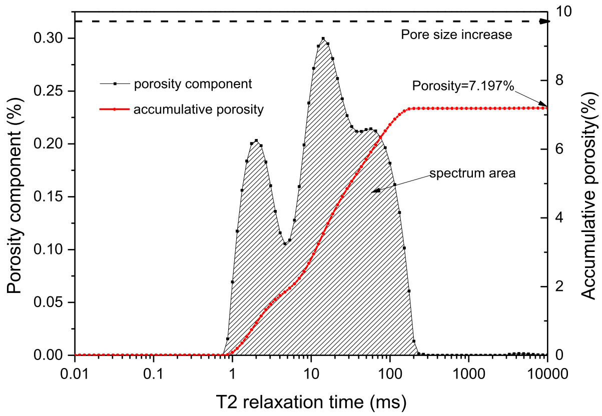

FIGURE 3. Method to calculate porosity.

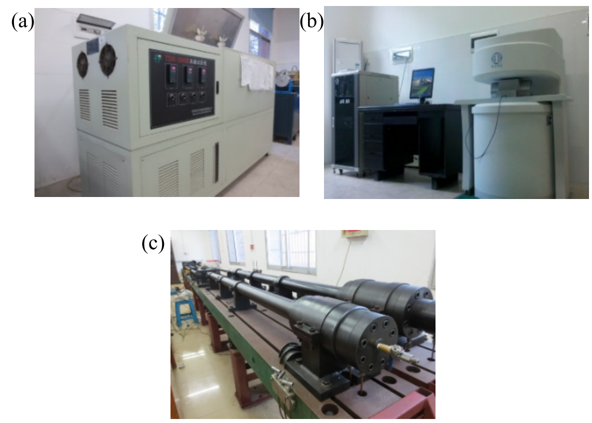

FIGURE 4. Test apparatus. (a) Cyclic F-T testing machine (b) NMR testing system (c) SHPB testing system.

The NMR tests were followed by dynamic compression tests conducted using a Splitting Hopkinson Pressure Bar (SHPB) to obtain the dynamic stress-strain curve for each specimen. The impact pressure of the SHPB test is 0.45MPa and the strain rate is about $75s^{-1}$.

C. TEST APPARATUS

A cyclic F-T testing machine (see Figure 4a), an NMR testing system (see Figure 4b) and an SHPB testing system (see Figure 4c) were used in this study.

III. PHYSICAL AND MECHANICAL RESULTS

A. POROSITY OF DETERIORATED SAMPLES

The porosity measured using the NMR system is shown in Figure 5. It was found that the porosity increases with the increase in the number of F-T cycles. The initial porosity of sandstone was 7.207%, and it increased to 11.4% when 140 F-T cycles were used. The main factor responsible for this increase in porosity is the temperature. During the F-T process, the frost heave force exceeds the bonding force between the mineral particles, which leads to the generation of new pores. The coefficient of correlation indicates good correspondence between the porosity and F-T cycles.

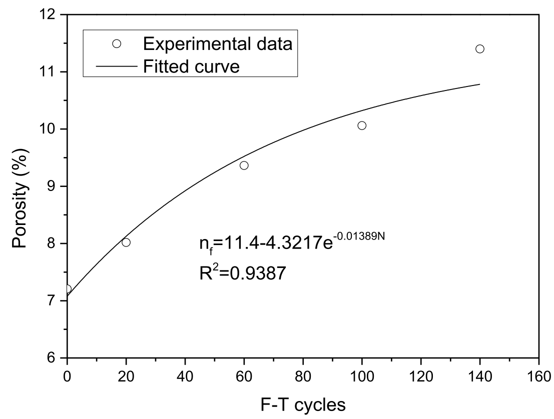

FIGURE 5. Correlation between F-T cycles and porosity.

B. DYNAMIC STRESS-STRAIN CURVES

Figure 6a presents the stress equilibrium during the impact test. Figure 6b shows the dynamic stress-strain curves of specimens under different F-T cycles, and Table 3 lists the statistical dynamic strength, Young's modulus and porosity. The data in Figure 6b and Table 3 demonstrates that the dynamic strength and Young's modulus decrease with the increase in the number of F-T cycles. The results were similar to those obtained in other research [43], [44]. It also demonstrated that the post-peak stress-strain characteristics exhibit two different behaviors based on the classification proposed by Wawersik and Fairhurst [9]. After the peak point, the rock samples first exhibit class I behavior and then class II behavior. This means that during the fracturing process, the rock samples transition from being ductile to brittle.

IV. PRE-PEAK AND POST-PEAK ENERGY-BASED BRITTLENESS INDEX

Figure 1 shows the classification of class I and class II behaviors. It can be seen that brittleness indices B_{10} [12] and B_{11} [19], which are based on pre-peak stress-strain relations, may be equal, even though the post-peak behavior

TABLE 3. Statistical results of mechanical and physical parameters.

F-T cycles	Porosity (%)	Dynamic strength/MPa	Young's modulus/GPa
0	7.207	95.9	16.14
20	8.018	88.5	13.76
60	9.362	83.4	12.20
100	10.06	79.1	11.26
140	11.4	72.7	10.50

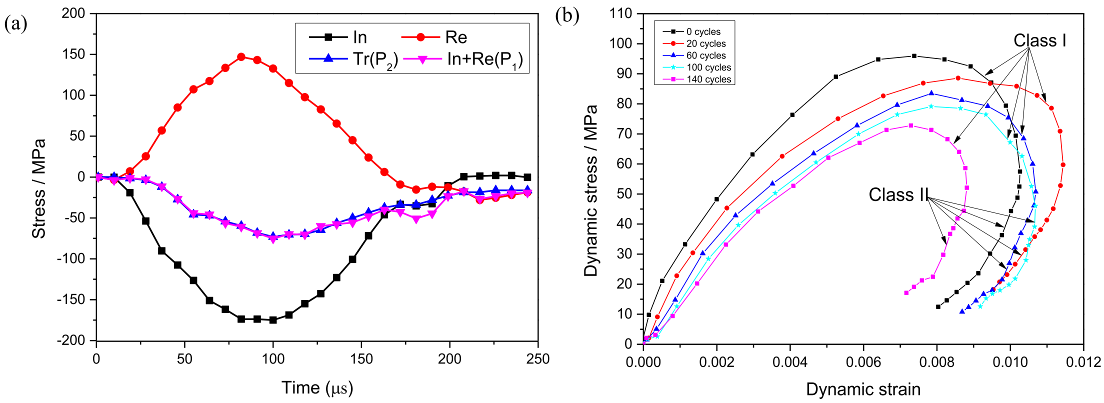

FIGURE 6. (a) stress equilibrium (b) dynamic stress-strain curves under different F-T cycles.

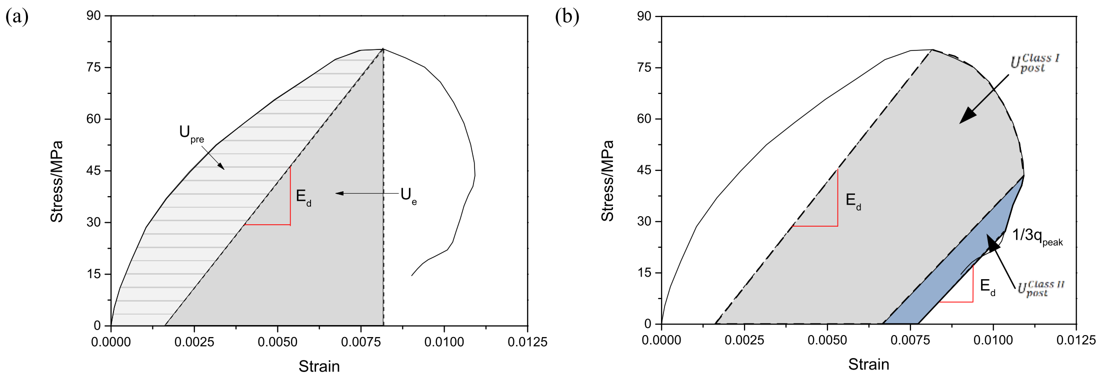

FIGURE 7. Strain energy of rock samples in dynamic compression.

was entirely different. Thus, it is necessary to take the post-peak stress-strain relations into consideration when defining a brittleness index.

The analysis described in the introduction shows that brittleness indices based on pre-peak behavior are not sufficient to describe the rock failure behavior. In addition, brittleness indices obtained from the static stress-strain relations are not sufficient to describe the rock failure behavior under impact load. As a result, two brittleness indices are proposed based on the pre-peak and post-peak dynamic stress-strain relations following energy balance to describe the rock behavior under impact load.

The elastic energy per unit volume of rock U_e^{peak} was evaluated by the area shown in Figure 7a. The post-peak energy was calculated using the unloaded pre-peak stress-strain curve and under the post-peak stress-strain as shown in Figure 7b. The post-peak energy is composed of the fracture energies consumed during class I and class II behaviors, and it is expressed by the following equation:

$$U_{post} = U_{post}^{ClassI} + U_{post}^{ClassII} \tag{1}$$

As presented in Figure 7b, an increase in energy consumed during class I behavior (i.e.U_{post}^{ClassI}) indicates the increase in brittleness. Conversely, an increase in the energy consumed during class II behavior (i.e.,$U_{post}^{ClassII}$) indicates the decrease in brittleness.

The following brittleness indices based on energy balance under impact load are proposed herein:

$$B_{U-1} = \frac{U_{post}^{ClassI}}{U_e^{peak}} \tag{2}$$

$$B_{U-2} = \frac{U_{post}^{ClassII}}{U_e^{peak}} \tag{3}$$

TABLE 4. Pre-peak and post-peak stress-strain quantities for the samples.

F-T cycles	U_{total}	U_{peak}	U_e^{peak}	U_{pre}	U_{post}	$U_{post}^{Class\ I}$	$U_{post}^{Class\ II}$	B_{U-1}	B_{U-2}
0	0.682	0.487	0.282	0.205	0.473	0.431	0.042	1.5445	0.1319
20	0.616	0.452	0.285	0.168	0.440	0.39	0.05	1.3995	0.147
60	0.579	0.432	0.285	0.147	0.427	0.371	0.056	1.3171	0.1811
100	0.554	0.382	0.256	0.125	0.422	0.361	0.061	1.1852	0.2142
140	0.380	0.323	0.217	0.107	0.266	0.192	0.075	0.9178	0.3124

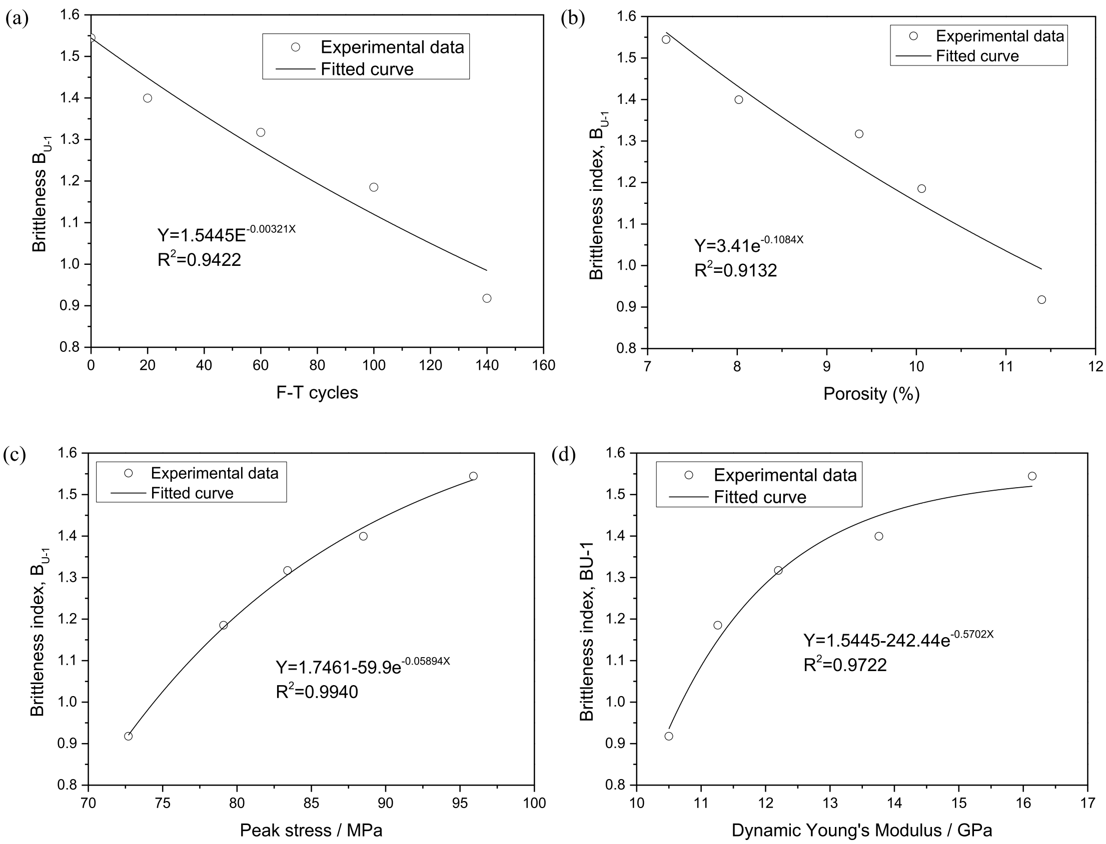

FIGURE 8. Correlation between brittleness index B_{U-1} and (a) F-T cycles, (b) porosity, (c) peak stress, (d) Young's modulus.

TABLE 5. Established relationships between brittleness indices and parameters.

Brittleness index	Parameter	Fitted curve	Decay constant	R^2
B_{U-1}	F-T cycles (N)	$B_{U-1} = 1.5445e^{-0.00321N}$	0.00321	0.9422
	Porosity (ρ)	$B_{U-1} = 3.41e^{-0.1084\rho}$	0.1084	0.9131
	Dynamic strength (q_{peak})	$B_{U-1} = 1.7461-59.9e^{-0.05894qpeak}$	0.05894	0.9940
	Dynamic modulus (E_d)	$B_{U-1} = 1.5445-242.44e^{-0.5702Ed}$	0.5704	0.9722
B_{U-2}	F-T cycles (N)	$B_{U-2} = 0.1319e^{0.00583N}$	0.00583	0.9651
	Porosity (ρ)	$B_{U-2} = 0.02421e^{0.2218\rho}$	0.2218	0.9670
	Dynamic strength (q_{peak})	$B_{U-2} = 6.74e^{-0.04279qpeak}$	0.04279	0.9429
	Dynamic modulus (E_d)	$B_{U-2} = 1.80e^{-0.1782Ed}$	0.1782	0.7693

where B_{U-1} and B_{U-2} are the two brittleness indices proposed in this paper, U_{post}^{ClassI} is the energy consumed during class I behavior, $U_{post}^{Class\ II}$ is the energy consumed during class II behavior. U_e^{peak} is the elastic energy stored in the specimen at the peak point. A larger value of B_{U-1} corresponds to a higher ductility of the rock. In contrast, a larger value of B_{U-2} indicates a more brittle rock.

Table 4 presents the pre-peak and post-peak stress-strain quantities for the samples, and the values of brittleness indices B_{U-1} and B_{U-2}. As shown in Table 4, the strain energy in both cases decreased to some extent with the increase in the number of F-T cycles, which means that the fracturing process required less energy if sandstone was deteriorated by the F-T cycles.

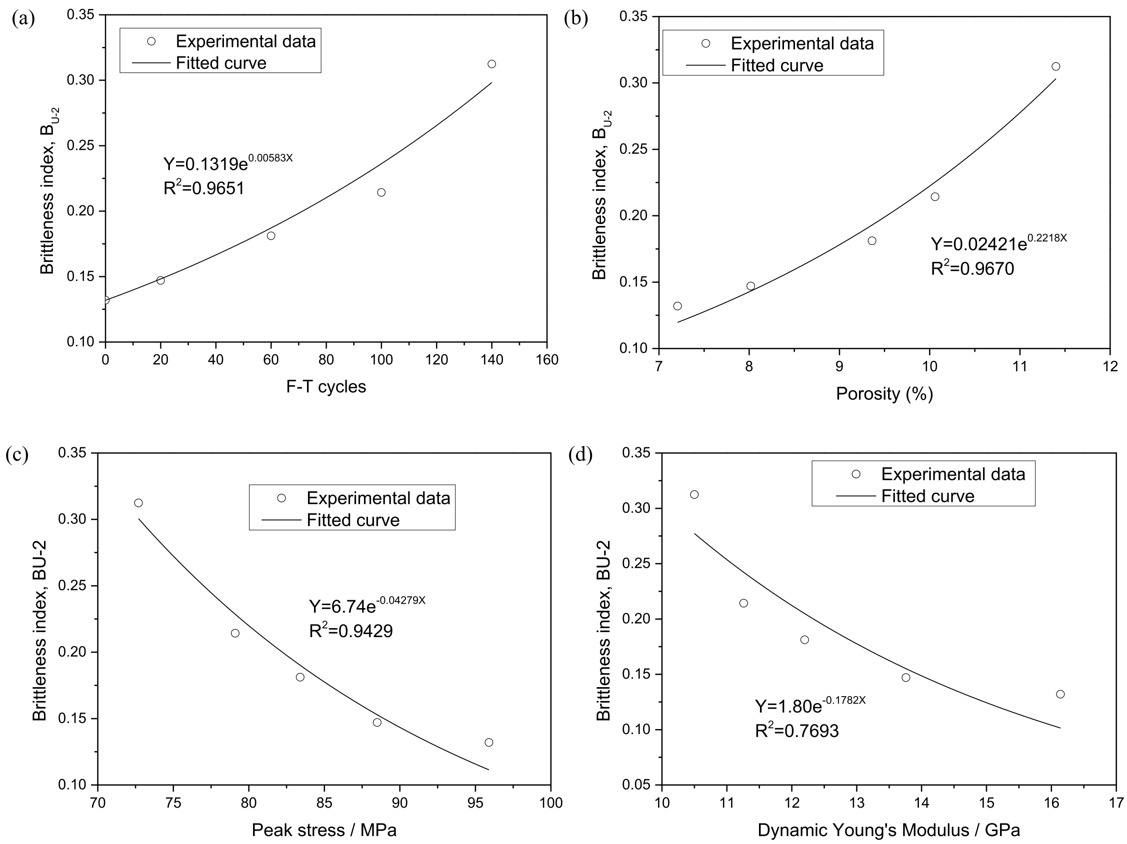

FIGURE 9. Correlation between brittleness index B_{U-2} and (a) F-T cycles, (b) porosity, (c) peak stress, (d) Young's modulus.

As demonstrated in Figures 8 and 9, the proposed brittleness indices B_{U-1} and B_{U-2} could describe the rock behavior properly. Brittleness B_{U-1} decreased in a nonlinear fashion with the increase in the number of F-T cycles and porosity, whereas B_{U-1} increased in a nonlinear manner with the increase in peak stress and Young's modulus. Brittleness B_{U-2} increased nonlinearly with increase in the number of F-T cycles and porosity, whereas B_{U-2} decreased nonlinearly with increase in peak stress and Young's modulus. This indicates that a larger number of F-T cycles lead to a lower brittleness B_{U-1} and a higher brittleness B_{U-2}, indicating a more brittle sandstone. From the results presented in Figures 8 and 9, a number of nonlinear relationships among the brittleness indices and F-T cycles, porosity, peak stress and Young's modulus were established and are presented in Table 5.

The results described above clearly demonstrate that the proposed brittleness indices are well correlated with F-T cycles, porosity, peak stress and Young's modulus. The results may thus be suitable for evaluating the drilling performance or the rock behavior under impact loads in cold regions.

V. CONCLUSION

In this study, two brittleness indices based on pre-peak and post-peak energy were proposed to characterize the rock behavior under F-T cycles and impact load. The porosity and dynamic stress-strain curves were determined by using an NMR testing system and SHPB apparatus. Two brittleness indices were proposed to characterize the rock behavior under impact loads after F-T cycles. The following conclusions can be drawn from this study.

a) The porosity increases while the dynamic strength decreases when F-T cycles applied.

b) Stress-strain results demonstrated that the sandstone samples showed a combined class I and class II behavior under impact loads after F-T cycles. It was also found that with the increase in F-T cycles the sandstone became more brittle.

c) The two proposed brittleness indices were strongly correlated with porosity, peak stress and Young's modulus. The results of this study suggest that the pre-peak and post-peak energy-based brittleness indices could be used as indicators for evaluating the rock behavior under F-T cycles and impact loads.

ACKNOWLEDGMENT

The authors also wish to thank Feng Bin for his help in undertaking the experimental tests.

REFERENCES

[1] R. Altindag, I. S Alyildiz, and T. Onargan, "Mechanical property degradation of ignimbrite subjected to recurrent freeze–thaw cycles," *Int. J. Rock Mech. Mining*, vol. 41, no. 6, pp. 1023–1028, 2004, doi: 10.1016/j.ijrmms.2004.03.005.

[2] M. Fener, and İ. İnce, "Effects of the freeze–thaw (F–T) cycle on the andesitic rocks (Sille-Konya/Turkey) used in construction building," *J. African Earth Sci.*, vol. 109, pp. 96–106, May 2015, doi: 10.1016/j.jafrearsci.2015.05.006.

[3] Z. Karaca, A. H. Deliormanli, H. Elçi, and C. Pamukcu, "Effect of freeze–thaw process on the abrasion loss value of stones," *Int. J. Rock Mech. Mining*, vol. 47, no. 7, pp. 1207–1211, 2010, doi: 10.1016/j.ijrmms.2010.07.003.

[4] A. Momeni, Y. Abdilor, G. R. Khanlari, M. Heidari, and A. A. Sepahi, "The effect of freeze–thaw cycles on physical and mechanical properties of granitoid hard rocks," *Bull. Eng. Geol. Environ.*, vol. 75, no. 4, pp. 1649–1656, 2015, doi: 10.1007/s10064-015-0787-9.

[5] D. T. Nicholson and F. H. Nicholson, "Physical deterioration of sedimentary rocks subjected to experimental freeze–thaw weathering," *Earth Surf. Process. Landforms*, vol. 25, no. 12, pp. 1295–1307, 2000. [Online]. Available: https://onlinelibrary.wiley.com/journal/10969837

[6] X. B. Li, T. S. Lok, and J. Zhao, "Dynamic characteristics of granite subjected to intermediate loading rate," *Rock Mech. Rock Eng.*, vol. 38, no. 1, pp. 21–39, 2004, doi: 10.1007/s00603-004-0030-7.

[7] L. M. Yang and V. P. W. Shim, "An analysis of stress uniformity in split Hopkinson bar test specimens," *Int. J. Impact Eng.*, vol. 31, no. 2, pp. 129–150, Feb. 2005, doi: 10.1016/j.ijimpeng.2003.09.002.

[8] Q. B. Zhang and J. Zhao, "Determination of mechanical properties and full-field strain measurements of rock material under dynamic loads," *Int. J. Rock Mech. Mining Sci.*, vol. 60, pp. 423–439, Jun. 2013, doi: 10.1016/j.ijrmms.2013.01.005.

[9] W. R. Wawersik and C. Fairhurst, "A study of brittle rock fracture in laboratory compression experiments," *Int. Int. J. Rock Mech. Mining Geomech. Abstr.*, vol. 5, no. 7, pp. 565–575, Sep. 1970, doi: 10.1016/0148-9062(70)90007-0.

[10] B. G. Tarasov and Y. Potvin, "Absolute, relative and intrinsic rock brittleness at compression," *Mining Technol.*, vol. 121, no. 4, pp. 218–225, 2013, doi: 10.1179/1743286312Y.0000000015.

[11] H. Munoz, A. Taheri, and E. K. Chanda, "Fracture energy-based brittleness index development and brittleness quantification by pre-peak strength parameters in rock uniaxial compression," *Rock Mech. Rock Eng.*, vol. 49, no. 12, pp. 4587–4606, 2016, doi: 10.1007/s00603-016-1071-4.

[12] V. Hucka and B. Das, "Brittleness determination of rocks by different methods," *Int. J. Rock Mech. Mining Sci. Geomech. Abstr.*, vol. 11, no. 10, pp. 389–392, 1974, doi: 10.1016/0148-9062(74)91109-7.

[13] C. He, S. Okubo, and Y. Nishimatsu, "A study of the class II behaviour of rock," *Rock Mech. Rock Eng.*, vol. 23, no. 4, pp. 261–273, 1990, doi: 10.1007/BF01043307.

[14] V. Hajiabdolmajid and P. Kaiser, "Brittleness of rock and stability assessment in hard rock tunneling," *Tunnelling Underground Space Technol.*, vol. 18, no. 1, pp. 35–48, 2003, doi: 10.1016/S0886-7798(02)00100-1.

[15] G. E. Andreev, *Brittle Failure of Rock Materials*. Boca Raton, FL, USA: CRC Press, 1995.

[16] A. W. Bishop, "Progressive failure with special reference to the mechanism causing it," in *Proc. Geotech. Conf.*, Oslo, Norway, 1967, pp. 142–450.

[17] R. Altindag, "The evaluation of rock brittleness concept on rotary blast hold drills," *J. Southern Afr. Inst. Mining Metall.*, vol. 102, no. 1, pp. 61–66, 2002. [Online]. Available: http://hdl.handle.net/10520/AJA0038223X_2763

[18] R. Altindag, "Relationships between brittleness and specific energy in excavation mechanics," in *Proc. Int. 9th Regional Rock Mech. Symp.*, Izmir, Turkey, 2008, pp. 427–451.

[19] A. Kidybiński, "Bursting liability indices of coal," *Int. J. Rock Mech. Mining Sci. Geomech. Abstr.*, vol. 18, no. 4, pp. 295–304, 1981, doi: 10.1016/0148-9062(81)91194-3.

[20] I. Batougina, "Methodological instructions for rockburst prophylaxis accounting the deposit geodynamics," Leningrad, VNIMI, Moscow, Russia, Tech. Rep., 1983.

[21] S. Bergman and H. Stille, "Rock burst problems in a 2.6 million M^3 underground crude oil storage in granite," in *Proc. 5th Int. Soc. Rock Mech. ISRM Congr.*, 1983, pp. 302–309.

[22] B. Manjikov, "Laboratory estimation of rockbursting danger," in *Proc. SSDRRMODMA, Frounze, Ilim*, 1983, pp. 16–106.

[23] I. Petoukhov and A. Linkov, *Mechanics of rockburst and outburst*, (in Russia). Moscow, Russia: Nedra, 1983.

[24] A. Stavroguin and A. Protossenia, "Rock strength and excavation stability in great depth," in *Proc. Nedra*, Moscow, Russia, 1985, p. 269.

[25] E. Rybacki, T. Meier, and G. Dresen, "What controls the mechanical properties of shale rocks?—Part II: Brittleness," *J. Petrol Sci. Eng.*, vol. 144, pp. 39–58, Aug. 2016, doi: 10.1016/j.petrol.2016.02.022.

[26] D. M. Jarvie, "Unconventional shale-gas systems: The Mississippian Barnett Shale of north-central Texas as one model for thermogenic shale-gas assessment," *AAPG Bull.*, vol. 91, no. 4, pp. 475–499, 2007, doi: 10.1306/12190606068.

[27] F. P. Wang and J. F. Gale, "Screening criteria for shale-gas systems," *Gulf Coast Assoc. Geol. Soc. Trans.*, vol. 59, pp. 779–793, 2009.

[28] J. C. Glorioso and A. J. Rattia, "Unconventional reservoirs: Basic petrophysical concepts for shale gas," in *Proc. SPE/EAGE Eur. Unconv. Resour. Conf. Exhib.-From Potential Prod.*, 2012, pp. 1–38.

[29] W. V. Grieser and J. M. Bray, "Identification of production potential in unconventional reservoirs," in *Proc. Prod. Oper. Symp.*, 2007, pp. 1–6. doi: 10.2118/106623-MS.

[30] R. Rickman, M. J. Mullen, J. E. Petre, W. V. Grieser, and D. Kundert, "A practical use of shale petrophysics for stimulation design optimization: All shale plays are not clones of the Barnett Shale," in *Proc. SPE Annu. Tech. Conf. Exhib.*, 2008, pp. 1–11, doi: 10.2118/115258-MS.

[31] X. Luan, "Laboratory measurements of brittleness anisotropy in synthetic shale with different cementation," in *Proc. SEG Tech. Program Expanded Abstr.*, 2014, pp. 3005–3009.

[32] S. Z. Sun, "Integrated prediction of shale oil reservoir using pre-stack algorithms for brittleness and fracture detection," in *Proc. Int. Petroleum Technol. Conf.*, 2013.

[33] Z. Guo, M. Chapman, and X. Li, "Exploring the effect of fractures and microstructure on brittleness index in the Barnett Shale," in *Proc. SEG Tech. Program Expanded Abstr.*, 2012, pp. 1–5.

[34] J. Chen, G. Zhang, H. Chen, and X. Yin, "The construction of shale rock physics effective model and prediction of rock brittleness," in *Proc. SEG Tech. Program Expanded Abstr.*, 2014, pp. 2861–2865.

[35] X. Jin, S. N. Shah, J.-C. Roegiers, and B. Zhang, "Fracability evaluation in shale reservoirs-an integrated petrophysics and geomechanics approach," in *Proc. SPE Hydraulic Fracturing Technol. Conf.*, 2014, pp. 1–14.

[36] S. Yagiz, "Assessment of brittleness using rock strength and density with punch penetration test," *Tunnelling Underground Space Technol.*, vol. 24, no. 1, pp. 66–74, 2009, doi: 10.1016/j.tust.2008.04.002.

[37] H. Munoz, A. Taheri, and E. K. Chanda, "Pre-peak and post-peak rock strain characteristics during uniaxial compression by 3D digital image correlation," *Rock Mech. Rock Eng.*, vol. 49, no. 7, pp. 2541–2554, Jul. 2016, doi: 10.1007/s00603-016-0935-y.

[38] Y. X. Zhou *et al.*, "Suggested methods for determining the dynamic strength parameters and mode—I fracture toughness of rock materials," *Int. J. Rock Mech. Mining Sci.*, vol. 49, pp. 105–112, Jan. 2012.

[39] A. Timur, "Pulsed nuclear magnetic resonance studies of porosity, movable fluid, and permeability of sandstones," *J. Petroleum Sci. Eng.*, vol. 21, no. 6, pp. 775–786, 1969, doi: 10.2118/2045-PA.

[40] S. Davies and K. J. Packer, "Pore-size distributions from nuclear magnetic resonance spin-lattice relaxation measurements of fluid-saturated porous solids. I. Theory and simulation," *J. Appl. Phys.*, vol. 67, no. 6, pp. 3163–3170, 1990, doi: 10.1063/1.345395.

[41] J. J. Howard and W. E. Kenyon, "Determination of pore size distribution in sedimentary rocks by proton nuclear magnetic resonance," *Mar. Petroleum Geol.*, vol. 9, no. 2, pp. 139–145, 1992, doi: 10.1016/0264-8172(92)90086-T.

[42] C. Straley, A. Matteson, S. Feng, L. M. Schwartz, W. E. Kenyon, and J. R. Banavar, "Magnetic resonance, digital image analysis, and permeability of porous media," *Appl. Phys. Lett.*, vol. 51, no. 15, pp. 1146–1148, 1987, doi: 10.1063/1.98766.

[43] Z. Zhou, X. Cai, L. Chen, W. Cao, Y. Zhao, and C. Xiong, "Influence of cyclic wetting and drying on physical and dynamic compressive properties of sandstone," *Eng. Geol.*, vol. 220, pp. 1–12, Mar. 2017, doi: 10.1016/j.enggeo.2017.01.017.

[44] P. Wang, J. Xu, X. Fang, and P. Wang, "Energy dissipation and damage evolution analyses for the dynamic compression failure process of red-sandstone after freeze-thaw cycles," *Eng. Geol.*, vol. 221, pp. 104–113, Apr. 2017, doi: 10.1016/j.enggeo.2017.02.025.

JIAN ZHANG (M'18) was born in Changsha, China, in 1988. He received the B.S. and M.S. degrees in mining engineering from Central South University. He is currently a Ph.D. candidate in rock mechanics with the School of Resources and Safety Engineering, Central South University, and also with The University of Adelaide. His research interests include rock mechanics and mining methods.

HONGWEI DENG received the B.S. degree in geological engineering, the M.S. degree in mining engineering, and the Ph.D. degree in safety engineering from Central South University. He is currently a Professor with Central South University. His research has been funded by many grants including the Natural Science Foundation of Hunan Province and the National Key Research and Development Plan. His research interests include mining method, disaster control technology, safety evaluation, and rock behavior in cold regions.

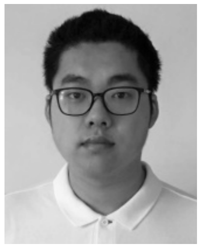

JUNREN DENG received the B.S. degree in mining engineering from the School of Resources and Safety Engineering, Central South University, Changsha, where he is currently pursuing the Ph.D. degree in mining engineering. His research interests include mining safety and rock mechanics.

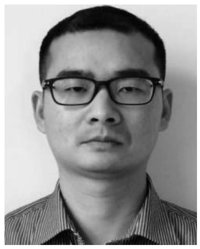

BO KE received the B.S. and M.S. degrees in mining engineering from the Wuhan University of Technology, Wuhan, and the Ph.D. degree in mining engineering from Central South University. He is currently an Academic Lecturer with the Wuhan University of Technology. His research interests include mining methods, borehole stability, and rock mechanics.